Attitude and Altitude Estimation for Quadrotor UAVs with a Moving Horizon Approach

Salvatore Rosario Bassolillo, Egidio D'Amato, Immacolata Notaro

***Abstract*—In the last decades, the growing use of low-cost electronics has pushed Unmanned Aerial Vehicles (UAVs) to general purpose audience in the civil sector. An accurate attitude and position estimation is crucial for a precise attitude and altitude control of this type of aircraft and represents a fundamental aspect to be taken into account. The main aim of this paper is to propose a Moving Horizon Estimator (MHE) able to fuse raw data coming from a set of sensors composed of an Inertial Measurement Unit (IMU), an optimal flow camera and several Time of Flight (ToF) distance sensors, oriented downward, with the scope of improving estimation performance in indoor or GPS-denied environment. The use of MHE allows to take into account constraints on state dynamics and noise features. To test the effectiveness of the proposed MHE algorithm, numerical simulations were conducted, evaluating the performance of the proposed algorithm in the presence of attitude maneuvers.**

***Index Terms*—Moving Horizon Estimation (MHE), Attitude estimation, sensor fusion, UAV navigation, quadrotor.**

I. Introduction

Unmanned Aerial Vehicles (UAVs) have gained significant attention due to their versatility and ease of use in a wide range of applications, from aerial surveillance to precision agriculture [1]–[8]. Indeed, compared to piloted aircraft, aerial drones offer advantages in terms of both cost and safety, providing support in dangerous or challenging environments. Multirotor UAVs, i.e. quadcopter, hexacopter, etc, have captured the attention of the general public; in fact, their ability to take-off and land vertically, flying in confined spaces and hovering over a specified area offers considerable advantages compared to fixed wing aircraft when used for missions in harsh and hazardous environments [9]. However, their operation requires accurate attitude and position estimation using only measurement from onboard sensors to enable the control system to effectively stabilize the vehicle. Currently, the most commonly employed sensors for UAV navigation are the Global Positioning System (GPS) [10] and the Inertial Navigation System (INS) [11] that usually incorporates an Inertial Measurement Unit (IMU) equipped with magnetic, angular rate, and gravity sensors (MARG). In particular, for small UAVs, IMUs are the preferred solution [12] for attitude estimation, being available in lightweight, low-cost and low power configurations [13], while offering relatively high performance.

Since attitude estimation relies on sensor accuracy and may be affected by the presence of rapid dynamics, integrating IMUs with additional types of sensors can be beneficial. Speed and position can also be determined through the integration of IMU and GPS sensors [14].

However, the use of GPS sensors requires the need to acquire information from satellites, making them effectively unusable in indoor or GPS-denied environments. In these scenarios, optical flow sensors have been widely adopted over the years [15]. Visual odometry is a bio-inspired solution, firstly introduced in 1950s by the scientist Gibson [16] to describe the visual perception of the world of such animals, considered as the projection of the 3D perceived motion of objects into a 2D plane. Since then, different solution that integrate optical flow technique with inertial measurement have been developed [17]–[19].

Over the years, the attitude estimation problem has been faced by finding several solutions. Complementary filters [20]–[22] represent the most commonly adopted techniques, thanks to their low computational costs and reliable estimation performance. However, issues related to accuracy, stability and sensitivity to local magnetic disturbances highlight the need to alternative approaches.

Several effective solutions are based on Kalman Filters (KF) [23], [24], Extended Kalman filters (EKF) [25], [26] and Unscented Kalman Filters (UKF) [27].

In scenarios featuring constraints on state variables or noise features, Kalman filtering may become sub-optimal or unstable. To mitigate these challenges, moving horizon estimation algorithm (MHE) represents a promising alternative. Indeed, this method allows to incorporate constraints into the online optimization problem solved at each time step over past observations, offering robustness against sudden changes in system dynamics [28]. MHE presents some conceptual similarities with Model Predictive Control (MPC), as both methods rely on optimization problems over a moving time horizon [29], [30]. Over the years various MHE schemes have been proposed in the literature for linear, non-linear, and hybrid systems [31]–[33].

This paper presents a MHE for the accurate attitude and altitude estimation of a quadrotor UAV, fusing raw data coming from one IMU, one downward oriented sonar and five downward oriented ultrasonic or Time of Flight (ToF) distance sensors, one placed at the center of the drone and the others at the end of each arm of the quadrotor. The aim of this

Salvatore Rosario Bassolillo and Egidio D'Amato are with the Department of Science and Technology, Universitá degli Studi di Napoli "Parthenope", Napoli, Italy; e-mail: salvatorerosario.bassolillo@collaboratore.uniparthenope.it (SRB), egidio.damato@uniparthenope.it (ED)

Immacolata Notaro is with the Department of Engineering, Universitá degli Studi della Campania "L. Vanvitelli", 81031, Aversa (CE), Italy; e-mail: immacolata.notaro@unicampania.it

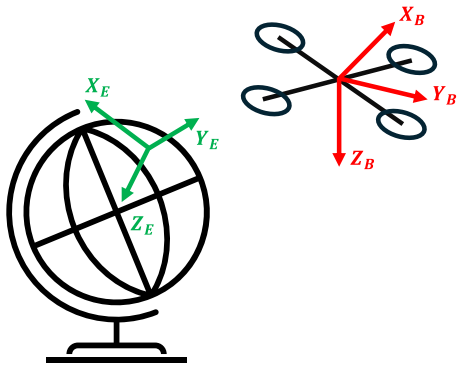

Fig. 1: Definitions of body and NED reference frames.

work is to show the improvement on the attitude and altitude estimation which can be obtained with the additional use of several downward faced distance sensors in different points of the structure, as well as the estimation of accelerations in fast maneuvers. Furthermore, the use of the MHE algorithm allowed to take into account constraints on state variables and noise characteristics. Some preliminary numerical results are provided to prove the effectiveness of the proposed scheme.

The paper is structured as follows: Section II describes the mathematical model employed to define the overall system dynamics, while Section III outlines the adopted MHE paradigm. Section IV presents the numerical results obtained by integrating the proposed MHE algorithm on a quadrotor dynamic simulator.

II. Reference Systems

Roll, pitch and yaw angle, are defined as the relative orientation between the body reference system and a fixed frame, as shown in Fig. 1. North-East-Down (NED) reference frame, denoted as E, is located on the surface of the Earth, with

- X_E-axis points north, parallel to the Earth surface;
- Y_E-axis points east, parallel to the Earth surface;
- Z_E-axis points downward, toward the Earth surface.

Body Reference Frame, denoted as B, is centered in the Center of Gravity (CG) of the quadrotor, with:

- X_B-axis points along the arm 1-2, positive forward;
- Y_B-axis points along the arm 2-3, positive rightward;
- Z_B-axis points downward, to form a right-handed reference frame.

The transformation from the NED reference frame to the body one can be achieved through a sequence of three successive rotations, using Euler angles, ϕ, θ, ψ:

- a rotation around the Z_E axis by the yaw angle ψ, from $OX_EY_EZ_E$ to $OX'Y'Z'$;
- a rotation around the Y' axis by the pitch angle θ from $OX'Y'Z'$ to $OX''Y''Z''$;
- a rotation around the X'' axis by the roll angle ϕ from $OX''Y''Z''$ to $OX_BY_BZ_B$.

The aforementioned Euler angles describe the aircraft's attitude. However, the unit quaternion, $\boldsymbol{q} = [q_0, q_1, q_2, q_3]^T$, offers an alternative representation to describe the attitude of a rigid body [34], avoiding singularities known as gimbal lock. In (1) is represented the correspondence between the quaternion and Euler angles:

$$\boldsymbol{q} = \begin{bmatrix} q_0 \\ q_1 \\ q_2 \\ q_3 \end{bmatrix} = \begin{bmatrix} \cos\frac{\phi}{2}\cos\frac{\theta}{2}\cos\frac{\psi}{2} + \sin\frac{\phi}{2}\sin\frac{\theta}{2}\sin\frac{\psi}{2} \\ \sin\frac{\phi}{2}\cos\frac{\theta}{2}\cos\frac{\psi}{2} - \cos\frac{\phi}{2}\sin\frac{\theta}{2}\sin\frac{\psi}{2} \\ \cos\frac{\phi}{2}\sin\frac{\theta}{2}\cos\frac{\psi}{2} + \sin\frac{\phi}{2}\cos\frac{\theta}{2}\sin\frac{\psi}{2} \\ \cos\frac{\phi}{2}\cos\frac{\theta}{2}\sin\frac{\psi}{2} - \sin\frac{\phi}{2}\sin\frac{\theta}{2}\cos\frac{\psi}{2} \end{bmatrix} \quad (1)$$

On the other hand, the Euler angles can be computed as follows [35]:

$$\phi = \arctan\left(\frac{2q_0q_1 + 2q_2q_3}{1 - 2q_1^2 - 2q_2^2}\right) \quad (2)$$

$$\theta = \arcsin\left(2q_0q_2 - 2q_3q_1\right) \quad (3)$$

$$\psi = \arctan\left(\frac{2q_0q_3 + 2q_1q_2)}{1 - 2q_2^2 - 2q_3^2}\right) \quad (4)$$

Let us introduce the rotation matrix associated to the unitary quaternion, needed to translate a vector from the NED reference to the body frame $\boldsymbol{q}$:

$$\boldsymbol{R_{BE}}(\boldsymbol{q}) = \begin{bmatrix} q_1^2 - q_2^2 - q_3^2 + q_0^2 & 2(q_1q_2 - q_3q_0) & 2(q_1q_3 + q_2q_0) \\ 2(q_1q_2 + q_3q_0) & -q_1^2 + q_2^2 - q_3^2 - q_0^2 & 2(q_2q_3 - q_1q_0) \\ 2(q_1q_3 - q_2q_0) & 2(q_2q_3 + q_1q_0) & -q_1^2 - q_2^2 + q_3^2 + q_0^2 \end{bmatrix} \quad (5)$$

III. Mathematical Model

Consider the following state vector

$$\boldsymbol{x}(t) = [\boldsymbol{q}(t)^T, \boldsymbol{V}_E(t)^T, z_E(t)]^T \quad (6)$$

where $\boldsymbol{V}_E$ represents the velocity vector the in reference frame at time t, and $z_E(t)$ is the altitude. The following mathematical relations describe the state dynamical model.

- The quaternion can be computed by integrating the angular velocity $\boldsymbol{\omega} = [p, q, r]^T$ from a known initial condition,

$$\dot{\boldsymbol{q}}(t) = \frac{1}{2}\boldsymbol{S}(\boldsymbol{\omega}(t)) \cdot \boldsymbol{q}(t) \quad (7)$$

  where $\boldsymbol{\omega}(t) = [p(t), q(t), r(t)]^T$ is angular velocity and $\boldsymbol{S}(\boldsymbol{\omega}(t))$ matrix is:

$$\boldsymbol{S}(\boldsymbol{\omega}(t)) = \begin{bmatrix} 0 & -p(t) & -q(t) & -r(t) \\ p(t) & 0 & r(t) & -q(t) \\ q(t) & -r(t) & 0 & p(t) \\ r(t) & q(t) & -p(t) & 0 \end{bmatrix} \quad (8)$$

- To estimate the velocity vector, the acceleration component not related to gravity $\boldsymbol{a}^B$ can be rotated in the inertial frame and integrated:

$$\dot{\boldsymbol{V}}^E(t) = \boldsymbol{R}_{\boldsymbol{BE}}^{\boldsymbol{T}}(\boldsymbol{q}(t)) \cdot \boldsymbol{a}^B(t) \quad (9)$$

- The altitude can be estimated by further integrating the velocity vector in the inertial frame.

$$\dot{z}^E(t) = [0, 0, 1] \cdot \boldsymbol{V}^E(t) \quad (10)$$

Consider a quadrotor equipped with the following devices:

- An IMU, composed by a gyroscope, an accelerometer and a magnetometer.
- An optical flow sensor, able to provide a 2D projection in the horizontal plane of the quadrotor 3D motion.
- Five ToF sensors, to measure the relative distance between each transmitter and the terrain.

At any time t, the measurement vector $\boldsymbol{y}(t)$ is:

$$\boldsymbol{y}(t) = [\boldsymbol{\omega}_s(t)^T, \boldsymbol{a_s}(t)^T, \boldsymbol{M}_s(t)^T, \boldsymbol{V}_S(t)^T, \boldsymbol{D}_s(t)^T] \quad (11)$$

where $\boldsymbol{\omega}_s(t)^(t)$ is the angular velocity vector measured by the gyroscope, $\boldsymbol{a_s}(t)^T$ is the accelerometer output, $\boldsymbol{M}_s(t)^T$ is a measure of Earth's magnetic field provided by the magnetometer, $\boldsymbol{V}_S(t)^T$ is provided by the optical flow device, and $\boldsymbol{D}_s(t)^T$ is the distance measured by ToFs. These measurements are affected by disturbances and noise.

The integration of measured angular velocity causes a drift in attitude estimation, known as the random walk effect. To mitigate this effect, measurements from accelerometers and magnetometers must be considered. However, accelerometers are particularly sensitive to structural vibrations, as well as magnetometer are sensitive to local disturbance in indoor environments, thus needing the fusion of data from multiple sensors to improve accuracy.

Analogously, the velocity vector cannot be obtained by simply integrating accelerometer data, since separating the non-gravitational acceleration component from the noise is challenging. For this reason, a reference can be obtained using a visual odometry-based sensor [18].

The measured angular velocity can be written as follows:

$$\boldsymbol{\omega}_s = \boldsymbol{\omega} + \boldsymbol{w}_g \quad (12)$$

where $\boldsymbol{w}_g(t) = [w_p(t), w_q(t), w_r(t)]^T$ represents a noise with unknown mean.

A tri-axial accelerometer measures forces, per unit mass, acting on the body along three specific orthogonal directions. For this reason, it can be used to measure the gravity acceleration on the rigid body.

$$\boldsymbol{a}_S^B(t) = \boldsymbol{R_{BE}}(\boldsymbol{q}(t)) \cdot \boldsymbol{g} + \boldsymbol{a}^B(t) + \boldsymbol{w_a}(t) \quad (13)$$

where the $\boldsymbol{w}_a$ includes a the disturbance and the noise $\boldsymbol{\nu_a}(t) = [\nu_{ax}(t), \nu_{ay}(t), \nu_{az}(t)]^T$

The local magnetic field direction can be measured through the magnetometer device as follows:

$$\boldsymbol{M}_S(t) = \boldsymbol{R_{BE}}(\boldsymbol{q}(t)) \cdot \boldsymbol{M}^E + \boldsymbol{\nu}_M(t) \quad (14)$$

where $\boldsymbol{\nu}_M(t) = [\nu_{Mx}(t), \nu_{My}(t), \nu_{Mz}(t)]^T$ represents the sensor noise vector.

At any time t, the optical flow provides a measure of a partial velocity vector in body frame:

$$\boldsymbol{V}_S(t) = \begin{bmatrix} u_S(t) \\ v_S(t) \end{bmatrix} = \begin{bmatrix} \frac{-u(t)\cdot\beta}{z^E(t)} - q(t)\cdot\beta + r(t)d_y(t) \\ \frac{-v(t)\cdot\beta}{z^E(t)} + p(t)\cdot\beta - r(t)d_x(t)(t) \end{bmatrix} + \boldsymbol{\nu}_O \quad (15)$$

where $u_S(t)$ and $v_S(t)]^T$ represent the velocity components in the body frame at time t, β is the focal length, $z^E(t)$ is the altitude of the UAV, $d_x(t)$ and $d_y(t)$ are the components in the horizontal plane of the distance vector between the center of gravity of the UAV and the camera, $\boldsymbol{\nu}_O = [\nu_{O_x}(t), \nu_{O_y}(t)]^T$ represents the sensor noise.

Finally the five ToFs provide the measurements about the distance from the UAV to the ground:

$$\boldsymbol{D}_S(t) = [d_{S,1}(t), d_{S,2}(t), d_{S,3}(t), d_{S,4}(t), d_{S,5}(t)]^T \quad (16)$$

with

$$d_{S,i}(t) = \frac{z_E}{\cos\phi(t)\cos\theta(t)} + \nu_{ToF_i}(t) \quad \forall i = 1, ..., 5 \quad (17)$$

where $\nu_{ToF_i}(t)$ is the sensor noise on the i-th device.

Denoting with $\boldsymbol{w} = [\boldsymbol{w}_g(t)^T \boldsymbol{w}_a(t)^T]^T$ the disturbance vector, and with $\boldsymbol{u} = \boldsymbol{\omega}$ the input vector, the state equations (7) (9) and (10) can be summarized as follows :

$$\dot{\boldsymbol{x}}(t) = \boldsymbol{\gamma}\left(\boldsymbol{x}(t), \boldsymbol{u}(t), \boldsymbol{w}(t)\right) \quad (18)$$

Similarly, exploiting (13), (14), (15) and (16), the measurement model can be expressed as:

$$\boldsymbol{y}(t) = \boldsymbol{g}(\boldsymbol{x}(t), \boldsymbol{u}(t), \boldsymbol{w}(t), \boldsymbol{v}(t)) \quad (19)$$

where $\boldsymbol{\nu}(t) = \left[\boldsymbol{\nu}_M(t)^T, \boldsymbol{\nu}_O(t)^T \boldsymbol{\nu}_{ToF}(t)^T\right]^T$ is the measurement noise vector.

Choosing a suitable sample time T_s, (18) and (19) can be converted in a time-discrete dynamics model:

$$\boldsymbol{x}(k) = \boldsymbol{f}\left(\boldsymbol{x}(k-1), \boldsymbol{u}(k-1), \boldsymbol{w}(k-1)\right) \quad (20)$$

$$\boldsymbol{y}(k) = \boldsymbol{g}\left(\boldsymbol{x}(k), \boldsymbol{u}(k), \boldsymbol{w}(k), \boldsymbol{\nu}(k)\right) \quad (21)$$

where k indicates the k-th sampling time instant, with $t_k = kT_S$.

IV. MHE Algorithm

The presence of disturbance and noise in (20) and (21) requires the use of a suitable fusion algorithm capable of estimating the disturbances and eliminating the noise contribution.

In this work, a MHE algorithm has been adopted. In MHE paradigm, the estimation of the state vector is achieved by solving a constrained optimization problem, considering the available measurements obtained over a n_t+1 steps time horizon: $\{k-n_t, k-n_t+1, ..., k\}$. At the same time, MHE allows to estimate the disturbance vector $\{\boldsymbol{w}(k-n_t|k) \dots \boldsymbol{w}(k|k)\}$ in the the considered time horizon.

In order to solve the problem with a quadratic programming algorithm, (20) and (21) are linearized around a reference point $(\tilde{\boldsymbol{x}}(\cdot), \tilde{\boldsymbol{u}}(\cdot), \tilde{\boldsymbol{w}}(\cdot))$ as follows:

$$\begin{aligned} \boldsymbol{\delta x}(k) =& \boldsymbol{A}(k-1)\boldsymbol{\delta x}(k-1) + \boldsymbol{B_u}(k-1)\boldsymbol{\delta u}(k-1) + \\ &+ \boldsymbol{B_w}(k-1)\boldsymbol{\delta w}(k-1) \end{aligned} \quad (22)$$

$$\boldsymbol{\delta y}(k) = \boldsymbol{C}(k)\boldsymbol{\delta x}(k) + \boldsymbol{D_u}(k)\boldsymbol{\delta u}(k) + \boldsymbol{D_w}(k)\boldsymbol{\delta w}(k) \quad (23)$$

where

$$\boldsymbol{\delta x}(k) = \boldsymbol{x}(\cdot) - \tilde{\boldsymbol{x}}(\cdot)$$
$$\boldsymbol{\delta u}(\cdot) = \boldsymbol{u}(\cdot) - \tilde{\boldsymbol{u}}(\cdot)$$
$$\boldsymbol{\delta w}(\cdot) = \boldsymbol{w}(\cdot) - \tilde{w}(\cdot)$$
$$\boldsymbol{\delta y}(\cdot) = \boldsymbol{y}(\cdot) - \tilde{\boldsymbol{y}}(\cdot)$$

with $\tilde{y}(\cdot) = \boldsymbol{g}(\tilde{\boldsymbol{x}}(\cdot)\tilde{\boldsymbol{y}}(\cdot)\tilde{\boldsymbol{y}}(\cdot), 0)$

$\boldsymbol{A}(k-1)$, $\boldsymbol{B_u}(k-1)$, and $\boldsymbol{B_w}(k-1)$ represent the Jacobian matrix of function $\boldsymbol{f}(\cdot)$ defined in (20) evaluated in the reference point at time instant $k-1$. Similarly, $\boldsymbol{C}(k)$, $\boldsymbol{D_u}(k)$, and $\boldsymbol{D_w}(k)$ represent the Jacobian matrix of function $\boldsymbol{g}(\cdot)$ defined in (21), evaluated in the reference point at time instant k.

At each time step k, the goal is to estimate the state vector $\hat{\boldsymbol{x}}(m|k)$, with $m = k-n_t, \ldots, k$, at the beginning of each time window by solving the MHE problem, defined as follows:

$$\Theta_k = \min_{[\widehat{\boldsymbol{\delta x}}(k-n_t|k), \{\widehat{\boldsymbol{\delta w}}(m|k)\}_{m=k-n_t}^{k-1}]} J_k \quad (24)$$

subject to the following constraints:

$$\overline{\boldsymbol{\delta x}}(m+1) = \boldsymbol{A}(k-1)\overline{\boldsymbol{\delta x}}(m) + \boldsymbol{B_u}(k-1)\boldsymbol{\delta u}(m) \quad (25)$$
$$\overline{\boldsymbol{\delta x}}(k-n_t-1) = \widehat{\boldsymbol{\delta x}}^*(k-n_t-1|k-1) \quad (26)$$
$$\widehat{\boldsymbol{\delta x}}(m+1|k) \in \mathbb{X} \quad (27)$$
$$\widehat{\boldsymbol{\delta w}}(m|k) \in \mathbb{W} \quad (28)$$

with $m = k-n_t, \ldots, k-1$. In (25) and (26) the dynamics of a priori estimate is defined $\overline{\boldsymbol{\delta x}}(m)$, whose initial condition represents the optimal solution $\widehat{\boldsymbol{\delta x}}^*(k-n_t-1|k-1)$ of the optimization problem at time step $k-1$.

In (25), $\boldsymbol{A}(k-1)$ and $\boldsymbol{B}(k-1)$ are evaluated in the point $(\widehat{\boldsymbol{x}}(k-n_t|k-1)^*, \boldsymbol{u}(k-n_t), \widehat{\boldsymbol{w}}(k-n_t|k-1)^*)$, where $\widehat{\boldsymbol{x}}(k-n_t|k-1)^* = \widehat{\boldsymbol{\delta x}}(k-n_t|k-1)^* + \widehat{\boldsymbol{x}}(k-n_t|k-2)^*$, and $\widehat{\boldsymbol{w}}(k-n_t|k-1)^* = \widehat{\boldsymbol{\delta w}}(k-n_t|k-1)^* + \widehat{\boldsymbol{w}}(k-n_t|k-2)^*$.

The cost function is

$$\begin{aligned} J_k = &\sum_{m=k-n_t}^{k-1} ||\widehat{\boldsymbol{\delta x}}(m|k) - \overline{\boldsymbol{\delta x}}(m)||^2_{\boldsymbol{Q}} \\ &+ \sum_{m=k-n_t}^{k} ||\boldsymbol{C}(k-1)\widehat{\boldsymbol{\delta x}}(m|k) - \boldsymbol{\delta y}_i(m)||^2_{\boldsymbol{O}} \\ &+ ||\widehat{\boldsymbol{\delta x}}(k-n_t|k) - \overline{\boldsymbol{\delta x}}(k-n_t)||^2_{\boldsymbol{P}} \end{aligned} \quad (29)$$

where the symbol $||\boldsymbol{e}||^2_{\boldsymbol{H}} = \boldsymbol{e}^T\boldsymbol{H}\boldsymbol{e}$ denotes a weighted quadratic error with respect to a matrix $\boldsymbol{H}$, and the matrix $\boldsymbol{C}(k-1)$ is evaluated in the point $(\widehat{\boldsymbol{x}}(k-n_t|k-1)^*, \boldsymbol{u}(k-n_t), \widehat{\boldsymbol{w}}(k-n_t|k-1)^*)$.

The objective function is the sum of three contributions: the first term addresses the state dynamics, weighted by a positive semi-definite matrix $\boldsymbol{Q}$, the second one accounts for the difference between measurements and model output, weighted by a positive definite matrix $\boldsymbol{O}$, corresponding to the inverse of noise measurement covariance, the last term takes into account the error between the estimated state $\widehat{\boldsymbol{\delta x}}(k-n_t|k)$ and the prediction $\overline{\boldsymbol{\delta x}}(k-n_t)$, resulting in an arrival cost, weighted by a suitable positive definite matrix $\boldsymbol{P}$ [31], [33], [36], [37].

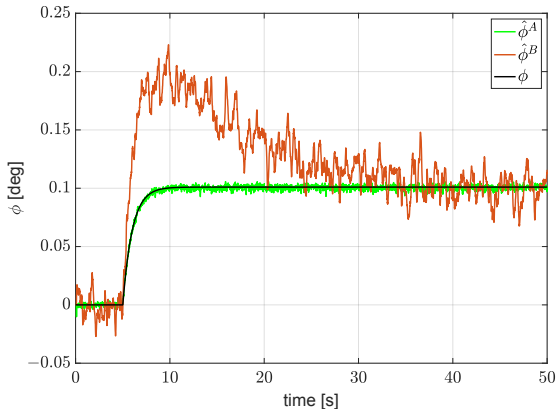

Fig. 2: Comparison of the estimate of the roll angle, ϕ, obtained using model A and model B with respect to the reference angle.

V. Numerical Results

In this Section, to assess the performance of the proposed algorithm, preliminary numerical results are presented, by simulating the quadrotor dynamics in Matlab/Simulink environment. The main simulation parameters are summarized in Table I.

The full suite of onboard sensors consists of one low-cost IMU, including a 3-axis accelerometer, a 3-axis gyroscope and a 3-axis magnetometer, one optical flow and five ToF sensors. The optical flow and the 5 distance sensors (4 placed at the end of each arm and one placed at the center of the structure) are oriented downwards in order to measure the velocity vector in the horizontal plane and the distance to the ground.

To prove the effectiveness of the full suite of onboard sensors in the attitude estimation, the simulation campaign takes into account two distinct quadrotor configurations, depending on the available onboard sensors:

A : 1 IMU, 1 optical flow sensor, 5 ToF sensors;
B : 1 IMU.

Simulation starts at $t = 0$ from an equilibrium condition in hovering at $h = 10m$ of altitude. To highlight the performance of the proposed estimation approach, several maneuvers are considered. In particular, distinct simulations were carried out by imposing step signals of 0.1rad at $t = 5$s around each axis (roll, pitch, and yaw). For altitude control, a ramp reference signal with a slope of 1m/s was applied at $t = 5$s, changing the altitude from $h = 10$m to $h = 11$m (see Table II).

Fig. 2 and Fig. 3 show the improvements obtained by the proposed technique, considering the sensor configuration A, over the classical INS quadrotor configuration B. Indeed, the attitude estimation considering quadrotor in configuration B

TABLE I: Quadcopter and sensors main parameters

Parameter	Value
Arm length - l $[m]$	0.7
Mass - m $[kg]$	1
Inertia tensor - J $[kg * m^2]$	$\text{diag}([5 * 10^{-2}, 5 * 10^{-2}, 10^{-1}])$
Gyroscope noise covariance - σ^2_{Gyro} $[(rad/s)^2]$	$6 * 10^{-6}$
Accelerometer noise covariance - σ^2_{Acc} $[(m/s^2)^2]$	$2.5 * 10^{-3}$
Magnetometer noise covariance - σ^2_{Mag} $[(G)^2]$	$2.5 * 10^{-7}$
Optical Flow noise covariance - σ^2_{OF} $[(m/s)^2]$	10^{-6}
ToF noise covariance - σ^2_{ToF} $[(m)^2]$	$2.6 * 10^{-7}$

TABLE II: Simulation Description

Simulation Type	**Imposed Signal**	**Applied Time (t)**	**Initial Value**	**Final Value**
Roll Maneuver	Step, 0.1 rad	5 s	0	0.1 rad
Pitch Maneuver	Step, 0.1 rad	5 s	0	0.1 rad
Yaw Maneuver	Step, 0.1 rad	5 s	0	0.1 rad
Altitude Change	Ramp, 1 m/s	5 s	10 m	11 m

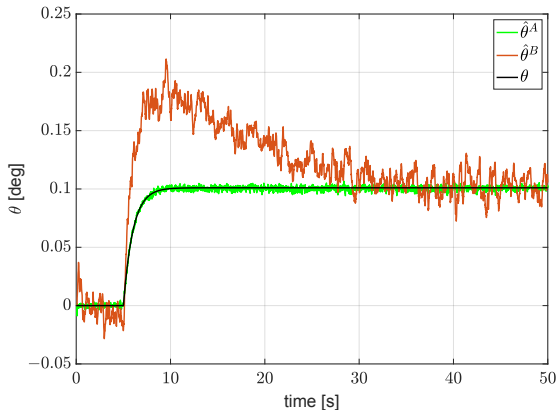

Fig. 3: Comparison of the estimate of the pitch angle, θ, obtained using model A and model B with respect to the reference angle.

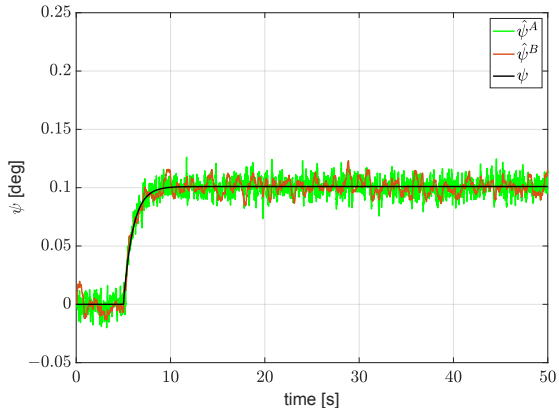

Fig. 4: Comparison of the estimate of the yaw angle, ψ, obtained using model A and model B, with respect to the reference angle.

causes the MHE to over-estimate pitch and roll angles due to the unobservable body accelerations measured during a maneuver.

In this regard, the possibility to place distance sensors in different points of the structure, as well as the possibility of estimate accelerations in fast maneuvers thanks to the presence of additional sensors, allows to solve these issues in pitch and roll estimation.

VI. Conclusions

In this paper, the design and testing of an attitude and altitude estimation algorithm based on MHE is presented. To improve the navigation performance provided by a typical suite of drone inertial sensors, such as accelerometers, gyroscopes and magnetometers, an optical flow camera and several ToF distance sensors have been used. The effectiveness of the proposed control algorithm has been tested through numerical simulations on a nonlinear quadcopter simulator, performing a sequence of attitude maneuvers around body axes, followed by a variation in altitude. Numerical results have proven the efficacy of the proposed estimation algorithm, comparing two different sensors configurations and highlighting the limitations of typical commercial sensor suites.

VII. Acknowledgement

This work was supported by the research project - ID:20222N4C8E "Resilient and Secure Networked Multivehicle Systems in Adversary Environments" granted by the Italian Ministry of University and Research (MUR) within the PRIN 2022 program, funded by the European Union through the PNRR program.

References

[1] S. A. H. Mohsan, M. A. Khan, F. Noor, I. Ullah, and M. H. Alsharif, "Towards the unmanned aerial vehicles (uavs): A comprehensive review," *Drones*, vol. 6, no. 6, p. 147, 2022.

[2] Z. Zaheer, A. Usmani, E. Khan, and M. A. Qadeer, "Aerial surveillance system using uav," in *2016 thirteenth international conference on wireless and optical communications networks (WOCN)*, pp. 1–7, IEEE, 2016.

[3] D. C. Tsouros, S. Bibi, and P. G. Sarigiannidis, "A review on uav-based applications for precision agriculture," *Information*, vol. 10, no. 11, p. 349, 2019.

[4] A. Skondras, E. Karachaliou, I. Tavantzis, N. Tokas, E. Valari, I. Skalidi, G. A. Bouvet, and E. Stylianidis, "Uav mapping and 3d modeling as a tool for promotion and management of the urban space," *Drones*, vol. 6, no. 5, p. 115, 2022.

[5] A. Ferraro and V. Scordamaglia, "Coordinated trajectory planning for ground-based multi-robot systems in exploration and surveillance missions," in *2023 IEEE International Workshop on Technologies for Defense and Security (TechDefense)*, pp. 131–136, IEEE, 2023.

[6] A. Ferraro, V. Nardi, E. D'Amato, I. Notaro, and V. Scordamaglia, "Multi-drone systems for search and rescue operations: problems, technical solutions and open issues," in *2023 IEEE International Workshop on Technologies for Defense and Security (TechDefense)*, pp. 159–164, IEEE, 2023.

[7] V. Scordamaglia, A. Ferraro, F. Tedesco, and G. Franzè, "Set-theoretic approach for autonomous tracked vehicles involved in post-disaster first relief operations," in *2024 10th International Conference on Control, Decision and Information Technologies (CoDIT)*, pp. 2006–2011, IEEE, 2024.

[8] A. Ferraro, C. De Capua, and V. Scordamaglia, "Integrated trajectory planning and fault detection for a skid-steered mobile robot deployed in post-disaster scenarios," in *2024 IEEE International Workshop on Technologies for Defense and Security (TechDefense)*, pp. 413–418, IEEE, 2024.

[9] A. Jaimes, S. Kota, and J. Gomez, "An approach to surveillance an area using swarm of fixed wing and quad-rotor unmanned aerial vehicles uav (s)," in *2008 IEEE International Conference on System of Systems Engineering*, pp. 1–6, IEEE, 2008.

[10] G. Flores, S. Zhou, R. Lozano, and P. Castillo, "A vision and gps-based real-time trajectory planning for a mav in unknown and low-sunlight environments," *Journal of Intelligent & Robotic Systems*, vol. 74, no. 1, pp. 59–67, 2014.

[11] A. Ali and N. El-Sheimy, "Low-cost mems-based pedestrian navigation technique for gps-denied areas," *Journal of Sensors*, vol. 2013, 2013.

[12] J. S. Jang and D. Liccardo, "Small uav automation using mems," *IEEE Aerospace and Electronic Systems Magazine*, vol. 22, no. 5, pp. 30–34, 2007.

[13] N. Barbour and G. Schmidt, "Inertial sensor technology trends," *IEEE Sensors journal*, vol. 1, no. 4, pp. 332–339, 2001.

[14] M.-D. Hua, "Attitude estimation for accelerated vehicles using gps/ins measurements," *Control engineering practice*, vol. 18, no. 7, pp. 723–732, 2010.

[15] Y. Lu, Z. Xue, G.-S. Xia, and L. Zhang, "A survey on vision-based uav navigation," *Geo-spatial information science*, vol. 21, no. 1, pp. 21–32, 2018.

[16] J. J. Gibson, "The perception of the visual world.," 1950.

[17] J.-C. Zufferey and D. Floreano, "Toward 30-gram autonomous indoor aircraft: Vision-based obstacle avoidance and altitude control," in *Proceedings of the 2005 IEEE International Conference on Robotics and Automation*, pp. 2594–2599, IEEE, 2005.

[18] C. Shen, Z. Bai, H. Cao, K. Xu, C. Wang, H. Zhang, D. Wang, J. Tang, and J. Liu, "Optical flow sensor/ins/magnetometer integrated navigation system for mav in gps-denied environment," *Journal of Sensors*, vol. 2016, 2016.

[19] Z. Yu, Y. Hu, and J. Huang, "Gps/ins/odometer/dr integrated navigation system aided with vehicular dynamic characteristics for autonomous vehicle application," *IFAC-PapersOnLine*, vol. 51, no. 31, pp. 936–942, 2018.

[20] S. O. Madgwick, A. J. Harrison, and R. Vaidyanathan, "Estimation of imu and marg orientation using a gradient descent algorithm," in *2011 IEEE international conference on rehabilitation robotics*, pp. 1–7, IEEE, 2011.

[21] M.-D. Hua, G. Ducard, T. Hamel, R. Mahony, and K. Rudin, "Implementation of a nonlinear attitude estimator for aerial robotic vehicles," *IEEE Transactions on Control Systems Technology*, vol. 22, no. 1, pp. 201–213, 2013.

[22] J. Wu, Z. Zhou, H. Fourati, R. Li, and M. Liu, "Generalized linear quaternion complementary filter for attitude estimation from multisensor observations: An optimization approach," *IEEE Transactions on Automation Science and Engineering*, vol. 16, no. 3, pp. 1330–1343, 2019.

[23] D. Gebre-Egziabher, R. C. Hayward, and J. D. Powell, "Design of multi-sensor attitude determination systems," *IEEE Transactions on aerospace and electronic systems*, vol. 40, no. 2, pp. 627–649, 2004.

[24] D. Choukroun, I. Y. Bar-Itzhack, and Y. Oshman, "Novel quaternion kalman filter," *IEEE Transactions on Aerospace and Electronic Systems*, vol. 42, no. 1, pp. 174–190, 2006.

[25] E. D'Amato, I. Notaro, M. Mattei, and G. Tartaglione, "Attitude and position estimation for an uav swarm using consensus kalman filtering," in *2015 IEEE Metrology for Aerospace (MetroAeroSpace)*, pp. 519–524, IEEE, 2015.

[26] R. Costanzi, F. Fanelli, N. Monni, A. Ridolfi, and B. Allotta, "An attitude estimation algorithm for mobile robots under unknown magnetic disturbances," *IEEE/ASME Transactions on Mechatronics*, vol. 21, no. 4, pp. 1900–1911, 2016.

[27] A. C. Chiella, B. O. Teixeira, and G. A. Pereira, "Quaternion-based robust attitude estimation using an adaptive unscented kalman filter," *Sensors*, vol. 19, no. 10, p. 2372, 2019.

[28] Q. S. Aolei Yang, Hao Wang and M. Fei, "Moving horizon estimation based on distributionally robust optimisation," *International Journal of Systems Science*, vol. 55, no. 7, pp. 1363–1376, 2024.

[29] F. Allgöwer, T. A. Badgwell, J. S. Qin, J. B. Rawlings, and S. J. Wright, "Nonlinear predictive control and moving horizon estimation—an introductory overview," *Advances in control: Highlights of ECC'99*, pp. 391–449, 1999.

[30] G. Franze, M. Mattei, L. Ollio, and V. Scordamaglia, "A robust constrained model predictive control scheme for norm-bounded uncertain systems with partial state measurements," *International Journal of Robust and Nonlinear Control*, vol. 29, no. 17, pp. 6105–6125, 2019.

[31] C. V. Rao, J. B. Rawlings, and J. H. Lee, "Constrained linear state estimation—a moving horizon approach," *Automatica*, vol. 37, no. 10, pp. 1619–1628, 2001.

[32] A. Alessandri, M. Baglietto, and G. Battistelli, "Receding-horizon estimation for discrete-time linear systems," *IEEE Transactions on Automatic Control*, vol. 48, no. 3, pp. 473–478, 2003.

[33] A. Alessandri, M. Baglietto, and G. Battistelli, "Moving-horizon state estimation for nonlinear discrete-time systems: New stability results and approximation schemes," *Automatica*, vol. 44, no. 7, pp. 1753–1765, 2008.

[34] R. G. Valenti, I. Dryanovski, and J. Xiao, "Keeping a good attitude: A quaternion-based orientation filter for imus and margs," *Sensors*, vol. 15, no. 8, pp. 19302–19330, 2015.

[35] J.-L. Blanco, "A tutorial on se (3) transformation parameterizations and on-manifold optimization," *University of Malaga, Tech. Rep*, vol. 3, p. 6, 2010.

[36] K. R. Muske, J. B. Rawlings, and J. H. Lee, "Receding horizon recursive state estimation," in *1993 American Control Conference*, pp. 900–904, IEEE, 1993.

[37] A. Alessandri, M. Baglietto, G. Battistelli, and V. Zavala, "Advances in moving horizon estimation for nonlinear systems," in *49th IEEE Conference on Decision and Control (CDC)*, pp. 5681–5688, IEEE, 2010.